THE JOURNAL OF PHYSICAL CHEMISTRY C

Article

pubs.acs.org/JPCC

Effects of Porphyrinic *meso*-Substituents on the Photovoltaic Performance of Dye-Sensitized Solar Cells: Number and Position of *p*-Carboxyphenyl and Thienyl Groups on Zinc Porphyrins

Ram Ambre,[†,‡] Kwan-Bo Chen,[†] Ching-Fa Yao,[‡] Liyang Luo,*[,†] Eric Wei-Guang Diau,*[,§] and Chen-Hsiung Hung*[,†]

[†]Institute of Chemistry, Academia Sinica, Nankang Taipei, 115 Taiwan

[‡]Department of Chemistry, National Taiwan Normal University, Taipei, 11677 Taiwan

[§]Department of Applied Chemistry and Institute of Molecular Science, National Chiao-Tung University, Hsinchu, 30010 Taiwan

Supporting Information

ABSTRACT: In order to understand the effects of *meso*-substituents of the zinc porphyrins on optical, electrochemical, and photovoltaic properties, a series of porphyrins with different combinations of thienyl (S) and *p*-carboxyphenyl (A) groups as the *meso* substituents have been systematically synthesized and studied. The properties of zinc complexes 3S1A, *trans*-2S2A, *cis*-2S2A, and 1S3A were fully investigated by absorption and emission spectra, attenuated total reflectance-Fourier transform infrared (ATR-FTIR) spectra, density functional theory (DFT) calculations, electrochemical, photophysical, and photovoltaic measurements. With the increasing number of *meso*-thienyl groups, slight red-shifts of Soret and Q bands were observed in both absorption and emission spectra. All of the absorption spectra of zinc porphyrins on TiO_2 film show broadening and splitting of Soret bands because of excitonic coupling of porphyrins. ATR-FTIR spectra revealed likely modes to determine either a single arm (in 3S1A and *trans*-2S2A) or double arms (in 1S3A and *cis*-2S2A) attached on TiO_2. Two factors of *p*-carboxyphenyl and thienyl groups affecting the devices performance—heavy atom effect and the amount of dye loading on TiO_2—are concluded. Overall, the power conversion efficiencies (η) of the devices exhibit the following order: 1S3A (3.0%) > *cis*-2S2A (2.5%) > *trans*-2S2A (1.8%) ≫ 3S1A (0.2%).

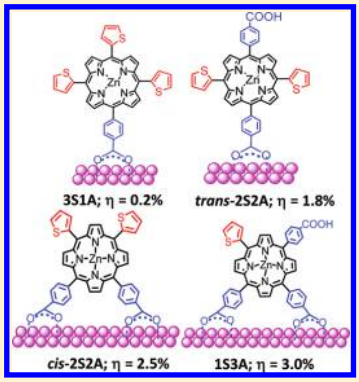

INTRODUCTION

In the wake of the global energy crisis, dye-sensitized solar cells (DSSC) are emerging as one of the most promising low-cost systems among all renewable-electricity generation technologies.[1,2] This system has offered dynamic research directions in the development of sensitizing dyes, controlling the morphology of nanocrystalline TiO_2, improvement on the behavior of electrolyte, and electrode fabrication. Among them, the design and synthesis of highly efficient photosensitizers have proved to be the most attractive but challenging tasks. During the past few years, tremendous efforts have been devoted to develop Ru-based complexes,[3,4] metal-free organic dyes,[5,6] and zinc porphyrins.[7−9] Among the investigated ruthenium sensitizers, N3, N719, black dye, and their derivatives have reported to be the most efficient compounds, having efficiencies up to 11.5%.[10−12] Nevertheless, the practical application of ruthenium-based dyes is obstructed by limited resources and high cost of ruthenium metal. Organic dyes have attracted much attention in recent years because of the ease of synthesis, possibility for a systematic structural modification, and low cost. To date, sensitizing dyes, including coumarin dyes,[13−15] indoline dyes,[16−19] carbazole dyes,[20,21] triarylamine dyes,[22−27] hemicyanine dyes,[28,29] squaraine dyes,[30] thiophene dyes,[31−33] and so forth, have been applied successfully in DSSCs with moderate efficiencies.

In view of its primary role in photosynthesis, porphyrins have been attractive for applying as sensitizers in DSSCs taking advantage of their strong Soret absorption and moderate absorption in the Q band region. In addition, the lowest unoccupied molecular orbital (LUMO) energy levels of porphyrins are generally well-situated above the TiO_2 conduction band (CB) for efficient electron injection, while the highest occupied molecular orbital (HOMO) levels are below the redox potential level of the I^-/I_3^- electrolyte for efficient dye regeneration. Moreover, it is revealed from photophysical measurements that the kinetics of electron injection from zinc porphyrin dyes into the TiO_2 band is indistinguishable from the reported highest efficiency ruthenium sensitizers.[34] Hundreds of porphyrin sensitizers have been synthesized and applied successfully in DSSCs.[7−9,11,35] A major breakthrough for the utilization of porphyrin dyes was synthesis of zinc porphyrins with a malonic acid substituted at the β-pyrrolic position, having an efficiency as high as 7.1%.[36] Lately,

Received: March 5, 2012
Revised: May 14, 2012
Published: May 14, 2012

   dx.doi.org/10.1021/jp302145x | J. Phys. Chem. C 2012, 116, 11907−11916

Chart 1. Molecular Structures of Zinc Porphyrins Used in This Study

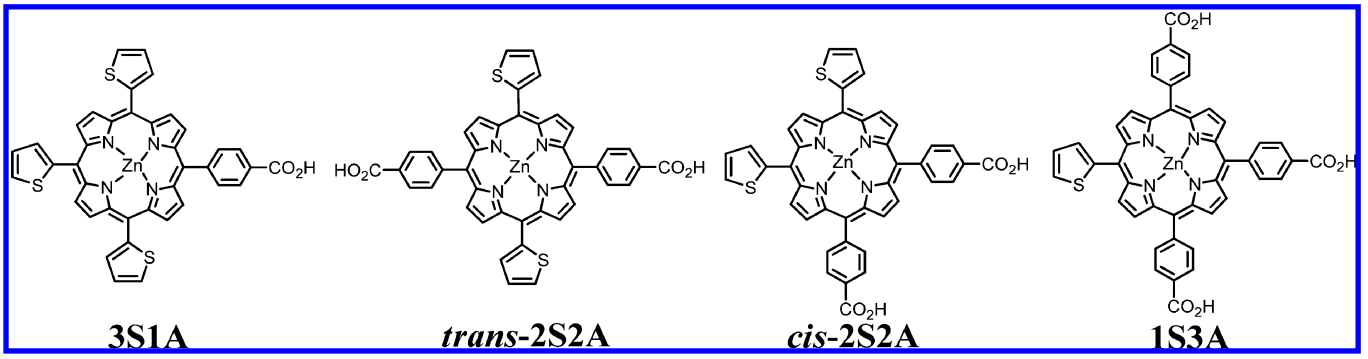

zinc porphyrins with a push−pull system (D-π-A) are becoming popular because of their ease of structural modifications on the electron-donating and anchoring sites, through which their optical, photophysical, and electrochemical properties might be tuned to attain a highly efficient DSSC device.[37−42] Recently, Grätzel, Diau, and Yeh et al. reported that the push−pull zinc porphyrin sensitizer YD2, with a diarylamino electron-donating group and ethynylbenzoic acid moiety serving as an electron-acceptor, demonstrated a η value of 11% under standard AM 1.5 one-sun illumination conditions, which is very close to the highest efficient ruthenium sensitizers.[38] In a very recent development, the specially designed D-π-A system incorporated YD2-*o*-C8 porphyrin sensitizer cosensitized with an organic dye using cobalt-based electrolyte leads to 12.3% efficiency under one-sun illuminations.[43]

The key factors affecting the overall solar energy conversion processes of porphyrin dyes can be grouped into (a) electronic structure of dyes,[44−47] (b) anchoring group of dyes,[45,48−50] (c) the bridging distance between dye and TiO_2,[51] (d) type of central metal,[50,52,53] and so forth. Currently, the most popular anchoring group used in sensitizing dyes is the carboxyl group, which has been known to bind to the TiO_2 surface tightly through a bidentate bridging mode.[50,51,54,55] Density functional theory (DFT) calculations have proved that the electronic structure of porphyrin will be strongly influenced by peripheral electron donating or electron withdrawing substituents.[56] Imahori et al. demonstrated that, although exhibiting lower overall light-harvesting efficiency (LHE), the light-harvesting properties were improved in the visible region for the *cis* or *trans bis*(diarylamino)-substituted zinc porphyrins.[48] Additionally, the electronic coupling between dye and TiO_2 conducting band is significantly influenced by anchoring the carboxyl group and alters the overall performance of the device. The effects on the number of carboxyl groups in ruthenium bipyridyl complexes of the photovoltaic properties have been systematically investigated.[57] Studies using ruthenium dyes as models suggested that at least two carboxyl groups are required for a strong binding with TiO_2 surface.[58,59] The most famous N3 ruthenium dye is known to anchor on TiO_2 through two of its carboxyl groups from the same or different bipyridyl ligands. Interestingly, not many porphyrins were reported with more than one carboxyphenyl group at *meso* or β-pyrrolic positions.[48,59−62] In this article we have synthesized a series of *meso*-thienyl and *meso*-*p*-carboxyphenyl-substituted zinc porphyrins, namely 3S1A, *trans*-2S2A, *cis*-2S2A, and 1S3A, bearing up to three carboxyl groups on a porphyrinic macrocycle, as represented in Chart 1. The electron rich thienyl, which can increase donor property and can provide better coplanarity to the porphyrin core than a phenyl group, has been used as the complementary *meso* substituent.[32,63,64] This systematic study, supported by optical spectra, cyclic voltammetry, DFT calculations, attenuated total reflectance-Fourier transform infrared spectroscopy (ATR-FTIR), and photovoltaic measurements, elucidates the significant influence of position and number of *p*-carboxyphenyl and thienyl groups on electronic structure and electrochemical and photovoltaic properties.

EXPERIMENTAL SECTION

Synthesis. The zinc porphyrins used in this study—3S1A, *trans*-2S2A, *cis*-2S2A, and 1S3A—were synthesized by the simplest possible route in three steps by literature reported methods. The mixed condensation of 4-methylformyl benzoate, 2-thiophenecarboxyaldehyde, and pyrrole in the presence of boron trifluoride-diethyl etherate as catalyst, followed by subsequent oxidation by 2,3-dichloro-5,6-dicyanobenzoquinone (DDQ) gave a mixture of six porphyrins, which were purified by column chromatography. Out of these six porphyrins, the four studied porphyrins were dissolved in CH_2Cl_2 and refluxed with zinc acetate in MeOH to obtain corresponding zinc complexes. The purification by column chromatography and subsequent hydrolysis by KOH isolated analytical pure products. All of the porphyrins were fully characterized by optical spectroscopy, ATR-FTIR, nuclear magnetic resonance spectroscopy, and high-resolution Fast atom bombardment (FAB) spectrometry. Detailed synthetic route and characterization data of all studied free base and zinc porphyrins are described in the Supporting Information.

Optical Spectroscopy. Transmittance and reflection UV−visible absorption spectra of the porphyrins in tetrahydrofuran (THF) and porphyrins absorbed on TiO_2 electrodes, respectively, were recorded using a JASCO V-670 UV−vis/NIR spectrophotometer. Steady-state fluorescence spectra were acquired by using a Varian Cary Eclipse fluorescence spectrophotometer.

Cyclic Voltammetry. The cyclic voltammetry measurements of all porphyrins were carried out on CHI 600D electrochemical analyzer (CH Instruments, Austin, TX, USA) in degassed THF containing 0.2 M tetrabutylammonium hexafluorophosphate (Bu_4NPF_6) as the supporting electrolyte. The cell assembly consists of a platinum working electrode, a Ag/AgCl reference electrode, and a platinum wire as the auxiliary electrode. The scan rate for all measurements was fixed at 100 mV/s. A ferrocene$^{+1/0}$ couple (0.56 V vs SCE) is used as the internal reference for correcting the applied potential.

dx.doi.org/10.1021/jp302145x | J. Phys. Chem. C 2012, 116, 11907−11916

Scheme 1. Synthesis of 3S1A, *trans*-2S2A, *cis*-2S2A, and 1S3A

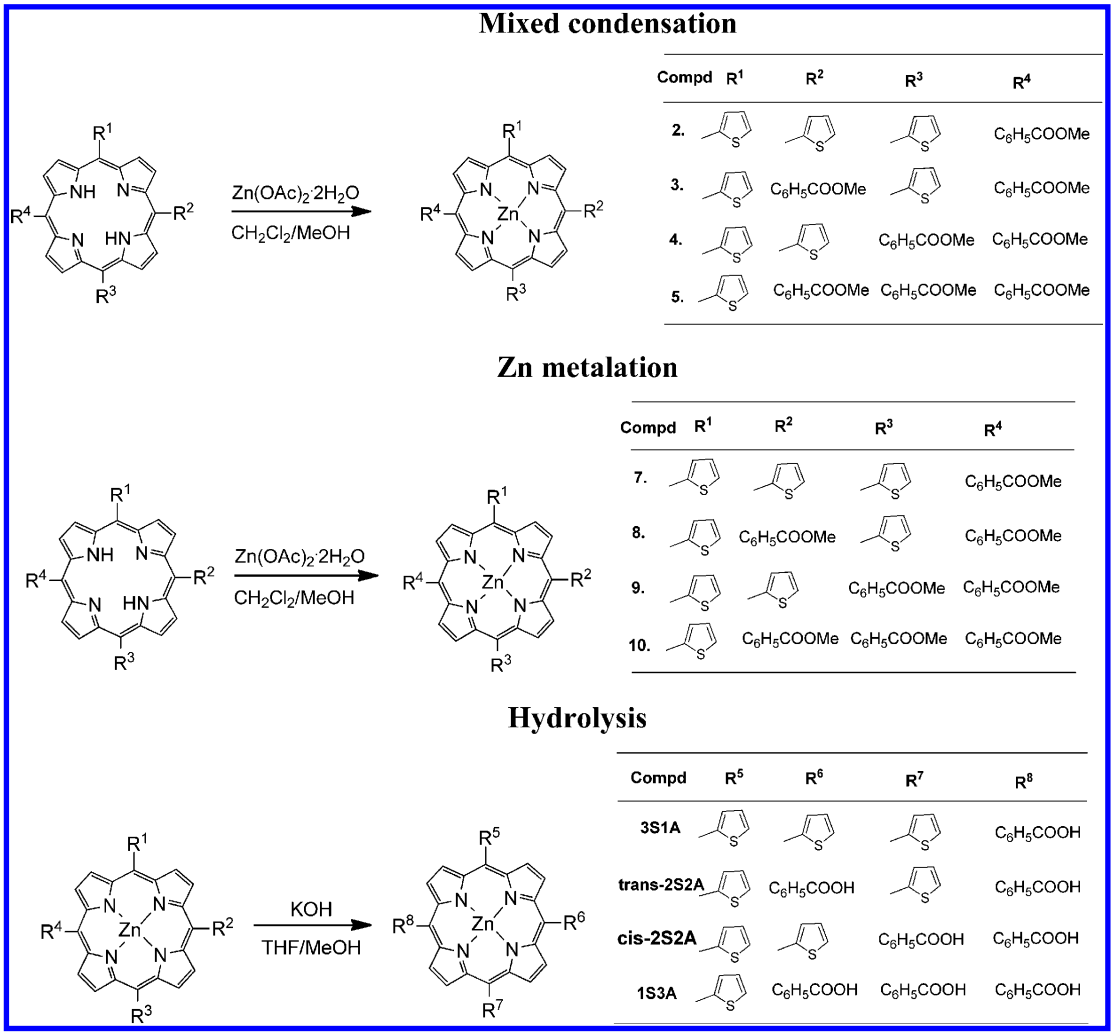

Fluorescence Lifetime Measurements. The picosecond fluorescence transients were measured with time-correlated single photon counting (PicoQuant, FluoTime 200). The samples were excited at 445 nm with a picosecond laser diode, and fluorescence decays were monitored at the maximum of fluorescence $Q(0,0)$ band for all zinc porphyrins (1×10^{-5} M) dissolved in atmospheric THF. The fluorescence lifetimes in THF solution were fit by single exponential function.

DFT Calculations. Geometry optimization and electronic structure of the porphyrins were performed with DFT (B3LYP) and the 6-31G* basis set in the Gaussian 03 program package.[65] The molecular orbitals were visualized by the Chemoffice software.

ATR-FTIR Measurements. ATR-FTIR spectra for the zinc porphyrins were recorded on a VERTEX 70 spectrometer by using Golden Gate diamond ATR accessory on solid powder of porphyrin samples. For the preparation of samples with zinc porphyrins absorbed on TiO_2, TiO_2 powder (5 mg) was mixed with 5 mL of zinc porphyrin solution (0.5 mM in dry THF) and kept for 12 h. Excess solvent were dropped out by pipet. TiO_2 powder was washed twice by THF and dried in vacuo, and the obtained powder sample was used for measurement. ATR-FTIR spectra for zinc porphyrin absorbed on TiO_2 were recorded at a resolution of 4 cm^{-1} and 320 scans.

Photovoltaic Measurements. To characterize the photovoltaic performance of the DSSC devices, a fluorine-doped tin oxide (FTO; 30 Ω/sq, Sinonar, Taiwan) glass (typical size 1.0 × 2.0 cm^2), used as a cathode, was coated with Pt particles by using the thermal platinum nanocluster catalyst method.[66] The Pt catalyst was deposited from a precursor solution composed of 5 mM solution of hexachloroplatinic acid in anhydrous isopropanol. The precursor solution was spin-coated on FTO glass (10 L/cm^2) and dried in air for 3 min. The coated Pt electrode was placed in an oven, and the temperature was gradually increased to 360 °C in 15 min. The porphyrin/TiO_2 layer was served as a working electrode (anode). We immersed the TiO_2-coated FTO (TiO_2 thickness 10 μm, active size 0.4 × 0.4 cm^2) in a THF solution containing 3S1A, *trans*-2S2A, *cis*-2S2A, and 1S3A (1×10^{-4} M) with 3×10^{-4} M of chenodeoxycholic acid (CDCA) at 40 °C for 3 h. To fabricate the DSSC device, the two electrodes were assembled into a sandwich-type cell, spaced, and sealed with a hot-melt film (SX1170, Solaronix, thickness 30 μm). The thin layer of electrolyte was introduced into the space between the two electrodes. A typical redox electrolyte contained lithium iodide (LiI, 0.1 M), diiodine (I_2, 0.01 M), 4-*tert*-butylpyridine (TBP, 0.5 M), 1-butyl-3-methylimidazolium iodide (BMII, 0.6 M), and guanidinium thiocyanate (GuNCS, 0.1 M) in a mixture of acetonitrile and valeronitrile (15/1, v/v).

dx.doi.org/10.1021/jp302145x | J. Phys. Chem. C 2012, 116, 11907−11916

The photocurrent and voltage curves were recorded with a digital source meter (Keithley 2400) under AM1.5 one-sun irradiation from a solar simulator (Sanei Electric XES-502S) calibrated with a Si-based reference cell (Hamamatsu S1133). The incident monochromatic photon-to-current conversion efficiency (IPCE) measurements were carried out with a home-built system, which includes a Xe lamp (PTi A-1010, 150 W), a monochromator (Dongwoo DM150i, 1200 gr/mm blazed at 500 nm), and a source meter (Keithley 2400). A standard Si photodiode (ThorLabs FDS1010) was used as a reference to calibrate the power density of the light source at each wavelength so that the IPCE of the DSSC device could be obtained.

RESULTS AND DISCUSSION

Synthesis. The synthetic procedures of 3S1A, *trans*-2S2A, *cis*-2S2A, and 1S3A are represented in Scheme 1. Condensation of pyrrole, methyl 4-formylbenzoate, and thiophene-2-carboxyaldehyde under Lindsey's conditions catalyzed by boron trifluoride-diethyl etherate followed by subsequent oxidation by DDQ afforded the mixture of six porphyrins. All six porphyrins were purified and characterized by various spectroscopic techniques. Each porphyrin can be distinguished by its unique splitting pattern in NMR spectroscopy. Noticeably, the *trans* and *cis* porphyrins, compounds **3** and **4** in Scheme 1, display characteristic splitting patterns for the resonances of β-pyrrolic protons. In the case of the *trans* product, eight protons on pyrrole rings split as 9.87 (d, J = 4.8 Hz, 4H), 8.87 (d, J = 4.8 Hz, 4H), whereas in the case of the *cis* product, four resonances, 9.08 (s, 2H), 9.07 (d, J = 4.8 Hz, 2H), 8.78 (d, J = 2.8 Hz, 2H), and 8.80 (s, 2H) were observed. The IR spectra of porphyrins show stretching frequency at around 1720 cm^{-1}, supporting the presence of ester carbonyl group. In the subsequent step, zinc metalation has been readily achieved in high yields by reacting free base porphyrin with zinc acetate. The success of zinc metalation was confirmed through the complete disappearance of the NMR resonance of inner NH with slight upfield shifts for all remaining protons. Hydrolysis of metal complexes has been achieved easily by reacting metal complexes in a mixture solution of THF and methanol with excess aqueous KOH. ATR-FTIR spectra of final acid products shows shifting of carbonyl peaks in the range of 1675−1700 cm^{-1} because of intermolecular hydrogen bonding.

Optical Spectroscopy. The UV−visible peak positions of the Soret and Q bands and the molar absorption coefficient (ε) of 3S1A, *trans*-2S2A, *cis*-2S2A and 1S3A in THF are listed in Table 1. The UV−visible spectra of the studied zinc porphyrins displayed in Figure 1 show typical metalloporphyrin features. Because of inductive effect from *meso*-thienyl unit, a slight red-shift in Soret and Q bands with the increase number of *meso*-thienyl groups has observed. Specifically, the 3S1A (428, 560, 600 nm) shows a red-shift over 1S3A (425, 558, 600 nm), whereas *trans*-2S2A (426, 560, 600 nm) and *cis*-2S2A (426, 560, 600 nm) exhibit comparable absorption wavelengths. Noticeably, the extinction coefficients in the Soret band region for the 1S3A and *trans*-2S2A are significantly higher than 3S1A and *cis*-2S2A. The steady-state fluorescence spectra of all zinc porphyrins measured in THF by excitation at the Soret band display a trend similar to the UV−visible spectra with significant red-shift upon increasing the number of *meso*-thienyl units.

To obtain the absorption spectra of the thin films, the TiO_2 films with coating thickness of around 1 μm were immersed in THF solutions of zinc porphyrins for 12 h and rinsed with THF to remove unabsorbed dye. The absorption spectra were recorded by reflectance measurements using an integrating sphere, and the results are shown in Figure 2. The UV−visible absorption spectrum of 3S1A/TiO_2 (magenta line) does not show any distinguishable change compared to its UV−visible absorption in THF due to weak binding of porphyrin with TiO_2, whereas UV−visible absorption spectra of *cis*-2S2A/TiO_2 (red line) and 1S3A/TiO_2 (black line) shifted to shorter wavelength because of H-type aggregation from face-to-face stacking of porphyrins and tight packing porphyrins on TiO_2.[67] The absorption spectra of porphyrins/TiO_2 demonstrate that the binding behavior of zinc porphyrin depends on the number and position of *p*-carboxyphenyl groups. When zinc porphyrins have more than two *p*-carboxyphenyl groups on the *meso* positions, the absorbance and molecular loading on TiO_2 are increased. Although the number of *p*-carboxyphenyl groups of *trans*-2S2A is the same as *cis*-2S2A, the amount of dye loading of *trans*-2S2A was lower than that of *cis*-2S2A because of single

Table 1. Optical and Electrochemical Data of Zinc Porphyrins in THF

dye	λ_{abs}/nm[a] (ε/10^3 M^{-1} cm^{-1})	λ_{em}/nm[b]	E_{OX}/V[c]	E_{0-0}/eV[d]	E_{OX}*/V[e]
3S1A	428 (248)	618	1.10	2.04	−0.94
	560 (10.7)	660			
	600 (3.0)				
trans-2S2A	426 (296)	613	1.11	2.05	−0.94
	560 (13.2)	660			
	600 (4.8)				
cis-2S2A	426 (243)	612	1.12	2.05	−0.93
	560 (10.7)	659			
	600 (3.4)				
1S3A	425 (352)	607	1.13	2.06	−0.93
	558 (14.5)	660			
	600 (4.8)				

[a]Absorption maximum of zinc porphyrin in THF. [b]Emission maximum measured in THF by exciting at the Soret band. [c]First oxidation potentials vs NHE determined using cyclic voltammetry in THF. [d]E_{0-0} values were estimated from the intersection of the absorption and emission spectra. [e]Excited state oxidation potentials approximated from E_{ox} and E_{0-0}.

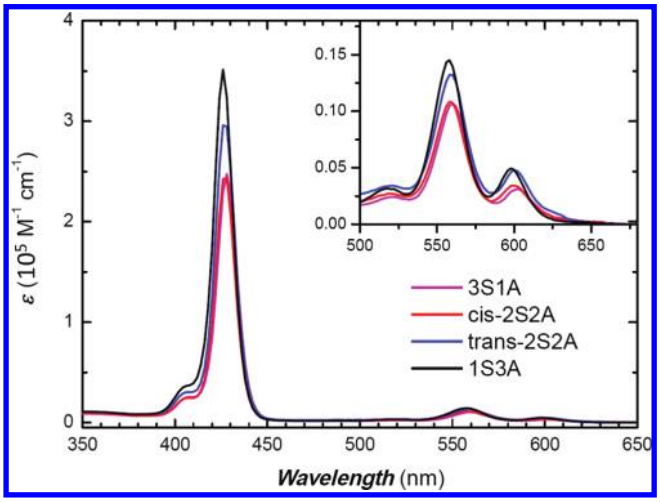

Figure 1. UV−visible spectra of 3S1A (magenta line), *trans*-2S2A (blue line), *cis*-2S2A (red line), and 1S3A (black line) in THF. Inset displays enlarged spectra for the Q-band absorptions.

dx.doi.org/10.1021/jp302145x | J. Phys. Chem. C 2012, 116, 11907−11916

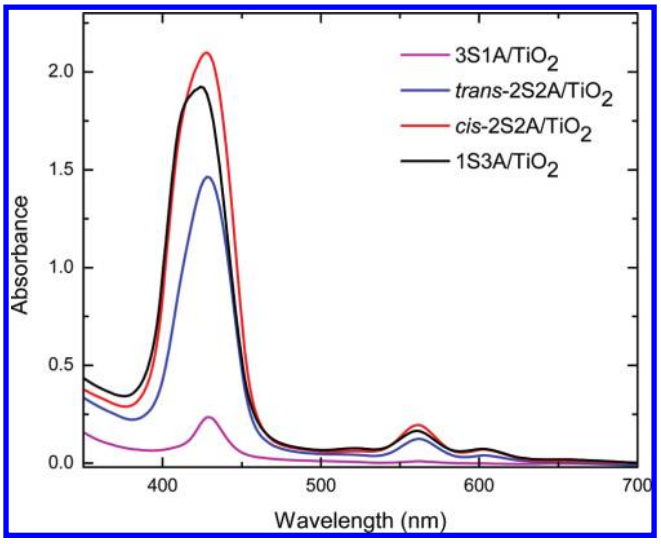

Figure 2. UV−visible spectra of 3S1A/TiO_2 (magenta line), *trans*-2S2A/TiO_2 (blue line), *cis*-2S2A/TiO_2 (red line), and 1S3A/TiO_2 (black line), immersed in 0.5 mM THF solution of zinc porphyrins for 12 h. The thickness of the TiO_2 films is ∼1 μm.

arm attachment on TiO_2 for the former, which is confirmed by the ATR-FTIR spectra (*vide infra*).

Cyclic Voltammetry. To determine the first oxidation potential (E_{OX}) of porphyrins, cyclic voltammetry measurements of zinc porphyrins containing 0.2 M $[Bu_4N]PF_6$ as the electrolyte were performed in degassed THF as displayed in Figure 3. The first oxidation couples of zinc porphyrins show reversible redox processes under a scan rate of 500 mV s^{-1}. As listed in Table 1, the 1S3A has the most positive first oxidation potential (1.13 V vs SHE) and the potential of 3S1A (1.10 V vs SHE) shows the most cathodic shift. The trend of redox potential is consistent with an overall effect from the electron withdrawing *meso*-*p*-carboxyphenyl and electron donating *meso*-thienyl. From the intersection of the normalized absorption and emission spectra at the *Q*(0,0) band (see Supporting Information Figure S1), the zero−zero excitation energies ($E_{0,0}$) were calculated to be 2.04, 2.05, 2.05, and 2.06 eV for 3S1A, *trans*-2S2A, *cis*-2S2A, and 1S3A, respectively. From the spectral and electrochemical measurements, the oxidation potential (E_{OX}*) with respect to the first singlet excited state of zinc porphyrins can be obtained and are listed in Table 1. The nearly identical E_{OX}* values of four zinc porphyrins indicate that the driving forces for electron injection from the excited zinc porphyrins to the CB of the TiO_2 films might be the same.

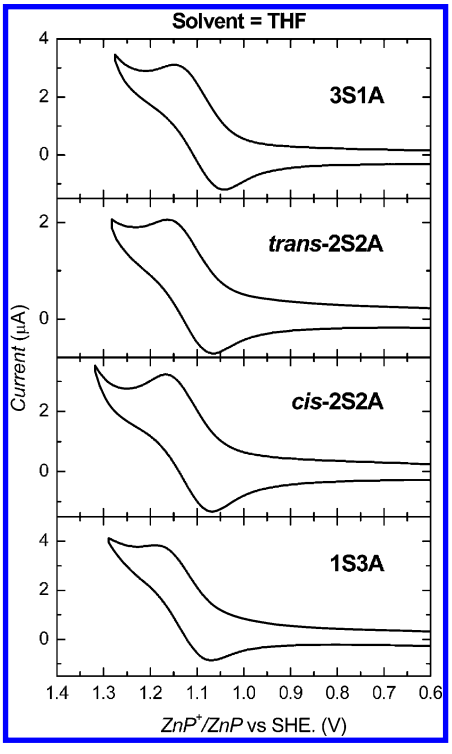

Figure 3. Cyclic voltammograms of 3S1A, *trans*-2S2A, *cis*-2S2A, and 1S3A in THF.

Fluorescence Lifetime Measurements. The fluorescence lifetimes of 3S1A, *trans*-2S2A, *cis*-2S2A, and 1S3A in THF were measured with the time-correlated single photon counting technique, and the results are displayed in Figure 4. The

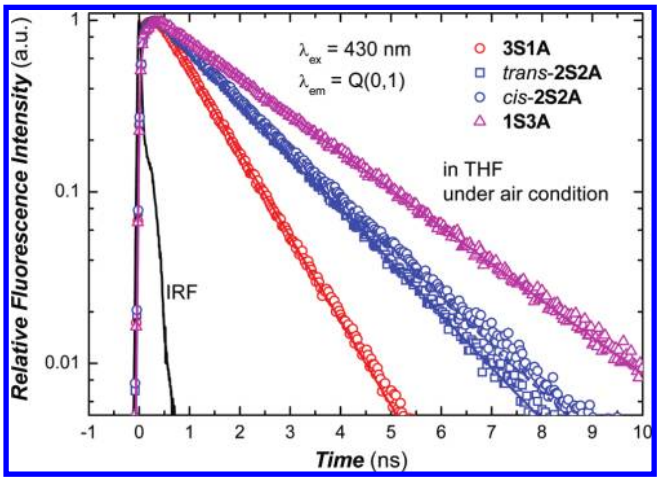

Figure 4. The ps-fluorescence transients of 3S1A (red circle), trans-2S2A (blue square), cis-2S2A (blue circle), and 1S3A (magenta triangle) in THF with excitation at 430 nm and monitoring at the *Q*(0,1) band. The black curve indicates the instrument response function (IRF).

samples in THF were excited at 430 nm (Soret band), and the fluorescence lifetimes were recorded at the maximum of fluorescence *Q*(0,1) band. All the fluorescence transients were fitted with a single exponential decay function to obtain lifetimes of 0.88 ± 0.02 ns for 3S1A, 1.49 ± 0.02 ns for *trans*-2S2A, 1.40 ± 0.02 ns for *cis*-2S2A, and 2.00 ± 0.02 ns for 1S3A. The excited state lifetimes of the zinc porphyrins decreasing with the increasing number of thienyl substituent group can be rationalized with the heavy atom effect of sulfur atoms, which increases the rate of intersystem crossing (ISC) upon increasing the number of sulfur atoms.

DFT Calculations. The ground state structures of 3S1A, *trans*-2S2A, *cis*-2S2A, and 1S3A were optimized using the hybrid B3LYP functional in combination with the standard 6-31G* basis set. Not only are the electron density distributions at the HOMO and LUMO orbitals of these porphyrins similar, but the energy gaps between LUMO and HOMO are also essentially identical (∼2.8 eV). These results are consistent with the relative insensitivity on the absorption spectra for all the substituted porphyrins. As shown in Figure 5 for the four zinc porphyrins at both the HOMO and LUMO orbitals, the π

dx.doi.org/10.1021/jp302145x | J. Phys. Chem. C 2012, 116, 11907−11916

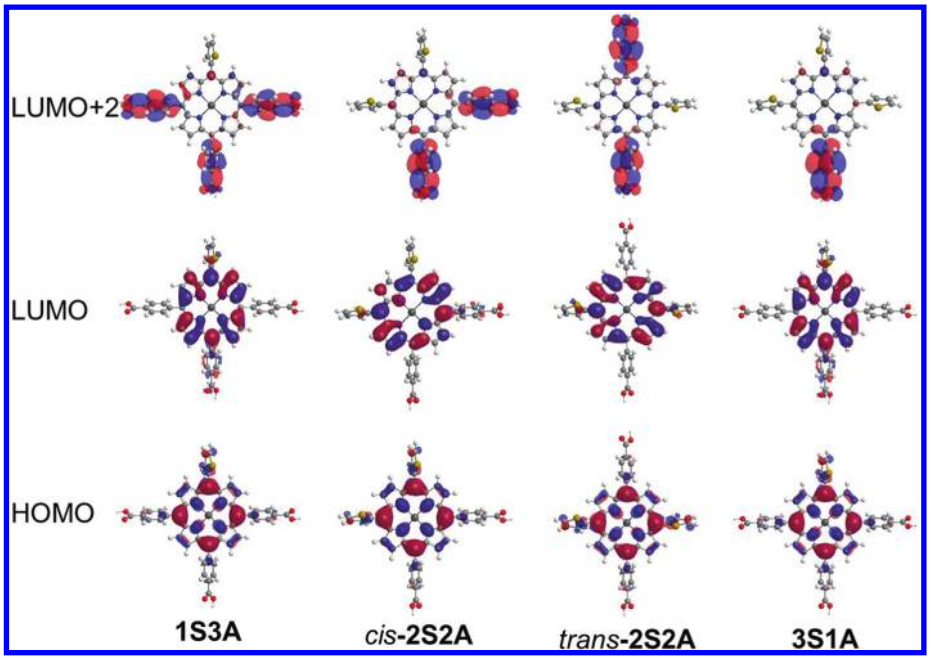

Figure 5. The molecular orbital diagrams of 3S1A, *trans*-2S2A, *cis*-2S2A, and 1S3A obtained from DFT calculations.

electron density distributions mainly localize at porphyrin-conjugated macrocycles. Since the *meso*-thienyl substituents and *meso*-*p*-carboxyphenyl are nearly orthogonal to the mean porphyrin planes, there is diminutive charge delocalization into terminal *meso*-*p*-carboxyphenyl moieties at LUMO and LUMO+1 orbitals. Interestingly, the anchoring *p*-carboxyphenyl possesses nearly exclusive electron density distributions at LUMO+2, suggesting that the electron injection from higher excited states involving LUMO+2 should be more efficient than the lower ones involving LUMO or LUMO+1.

Dye Loading Measurements. To understand the adsorption behavior and quantify the amount of dye loading, we examined the porphyrin densities (Γ) adsorbed on TiO_2 surface. The TiO_2 electrodes of 10 μm thickness were immersed in 0.1 mM zinc porphyrin THF solution containing 0.3 mM CDCA for 3 h at 40 °C. No desorptions of *cis*-2S2A and 1S3A were observed when the dye-sensitized TiO_2 plates were rinsed with THF, indicating the tight bonding of dyes to the TiO_2 surface. On the contrary, 3S1A and *trans*-2S2A were readily desorbed from TiO_2 which signifies a weak interaction with TiO_2. The porphyrin density (Γ) adsorbed on the rinsed TiO_2 film was determined by measuring the absorbance of the zinc porphyrins that were desorbed from the sensitized TiO_2 films after being immersed in 0.1 M KOH solution in THF. The saturated Γ values of porphyrins were determined as 83 ± 10, 110 ± 4, 126 ± 5, and 117 ± 1 nmol cm^{-2} for 3S1A, *trans*-2S2A, *cis*-2S2A, and 1S3A, respectively. The Γ values of these porphyrins are comparatively higher than those of reported *meso*-aryl-substituted zinc porphyrins.[48,67]

ATR-FTIR Spectroscopy. We have applied ATR-FTIR spectroscopy as the prime tool to evaluate the number and mode of porphyrinic *p*-carboxyphenyl attached on TiO_2.[54,65,67−69] The ATR-FTIR spectra of zinc porphyrin powder samples are contrasted with the spectra of zinc porphyrin adsorbed on TiO_2 and demonstrated in Figure 6. The spectra of 3S1A, trans-2S2A, cis-2S2A, and 1S3A in powder form exhibit very strong ν(C═O) stretching peaks at 1675, 1681, 1687, and 1680 cm^{-1}, respectively. The ν(C═O) peak at 1675 cm^{-1} observed in the 3S1A powder disappeared completely in the corresponding spectrum of the 3S1A/TiO_2 film, while strong absorptions at 1650 and 1400 cm^{-1}, assigned as $\nu_{asym}(COO^-)$ and $\nu_{sym}(COO^-)$, respectively, were observed. The energy difference of the $\nu_{asym}(COO^-)$ and $\nu_{sym}(COO^-)$ suggests a bidentate bridging or bidentate chelating *p*-carboxyphenyl group coordinated to TiO_2. A similar pattern can be observed for the ATR-FTIR spectra of cis-2S2A/TiO_2, suggesting both the *p*-carboxyphenyl groups attached on TiO_2.[48,68,70] On the contrary, the ATR-FTIR spectra of *trans*-2S2A/TiO_2 shows marked increase in $\nu_{asym}(COO^-)$ and $\nu_{sym}(COO^-)$ whereas the ν(C═O) stretching peak at 1681 cm^{-1} is still present with significant absorbance, suggesting the presence of a free unchelated *p*-carboxyphenyl unit. The comparative ATR-FTIR spectrum of 1S3A/TiO_2 shows more intense absorptions for $\nu_{asym}(COO^-)$ and $\nu_{sym}(COO^-)$ than that of ν(C═O), suggesting that out of three *p*-carboxyphenyl groups one is free and two are involved in attachment with TiO_2. The results of dye-loading and the photovoltaic properties (*vide infra*) are consistent with those of the ATR-FTIR study, suggesting that the presence of two *meso*-*p*-carboxyphenyl at the *cis* position in *cis*-2S2A and 1S3A gives stronger attachment to TiO_2 and results in better device performances than those of 3S1A and *trans*-2S2A with only a single arm attached to the TiO_2.

Photovoltaic Measurements. The photocurrent−voltage (*I*−*V*) curves of 1S3A, *trans*-2S2A, *cis*-2S2A, and 3S1A under AM 1.5 solar simulator light and in the dark are shown in Figure 7. Significant differences for the short-circuit current densities (J_{SC}), the open-circuit voltages (V_{OC}) and the power conversion efficiency (η) of the devices were observed. It is noticed that the values of both J_{SC} and V_{OC} are systematically increased with increasing number of bonding *meso*-*p*-carboxyphenyl on TiO_2 and decreasing number of *meso*-thienyl substituent. The efficiencies of 1S3A and *cis*-2S2A with double arms attached on TiO_2 are higher than those of *trans*-2S2A and 3S1A with only a single arm attached on TiO_2. Due to the maximum number of coordinating *meso*-*p*-carboxyphenyls and

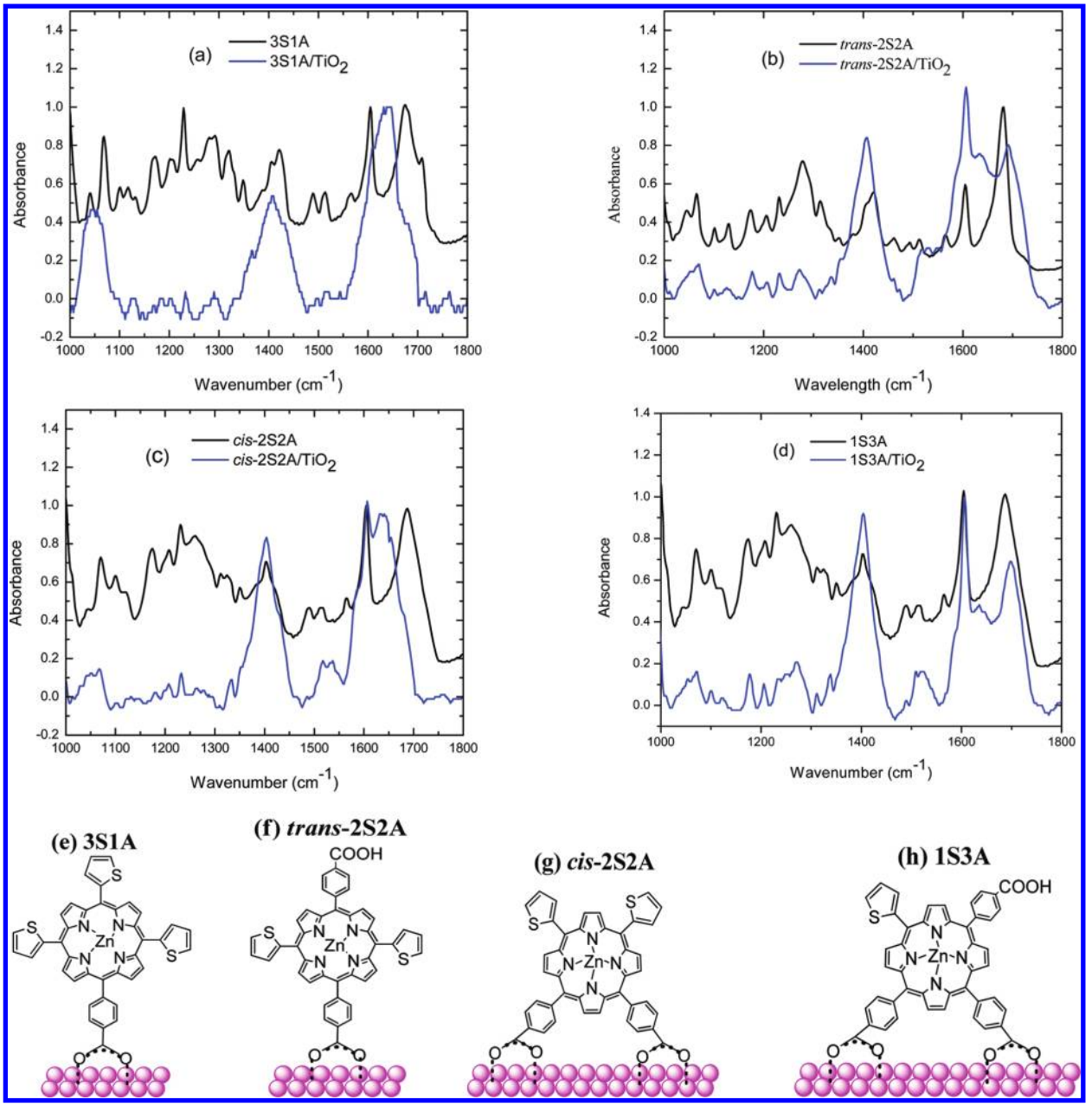

Figure 6. ATR-FTIR spectra of zinc porphyrins in powder form (black line) and zinc porphyrins on TiO_2 (blue line) for (a) 3S1A, (b) *trans*-2S2A, (c) *cis*-2S2A, and (d) 1S3A. ATR-FTIR spectra of porphyrins on TiO_2 are normalized for comparison. Possible modes of attachment of zinc porphyrins on TiO_2 are illustrated for (e) 3S1A, (f) *trans*-2S2A, (g) *cis*-2S2A, and (h) 1S3A. For demonstration purposes, relative sizes of molecules and nanoparticles are not correlated in real dimensions.

minimum heavy atom effect, 1S3A gives the highest efficiency. As demonstrated in Figure 7 and Table 2, a significant difference on V_{OC} values was observed to give the order 1S3A > *cis*-2S2A ~ *trans*-2S2A > 3S1A. In general, the V_{OC} value is determined by the difference between the Fermi level of electrons on TiO_2 and potential level of redox couples in electrolyte. Because the potential level of redox couples in our system is the same, the values of V_{OC} are dependent on the Fermi levels of electrons on TiO_2 after electron injection for all the porphyrin systems. Since both 1S3A and *cis*-2S2A devices have greater J_{SC} values than those of the *trans*-2S2A and 3S1A devices, it is expected that the dual-arm anchored devices have more injected electrons on the CB of TiO_2 to give higher Fermi levels than those of the single-arm anchored devices, which explains the general trend in the variation of V_{OC}. On the other hand, the much higher V_{OC} and J_{SC} for 1S3A than *cis*-2S2A reflect a better performance for the dye containing less thienyl groups. Under the circumstance that 1S3A and *cis*-2S2A have near identical dye loadings and the same chelating mode, the heavy atom effect appears to decrease the conversion efficiency of *cis*-2S2A through, presumably, increasing the rate of ISC, as has been observed from the fluorescence lifetime measurements. On the basis of the $I-V$ curves obtained in the dark (Figure 7b), an increase in the number of *meso*-*p*-carboxyphenyl substituent is accompanied with a lower dark current density. Because the dark current density is governed by the impedance of the electron transfer between TiO_2 and electrolyte, the adsorbed porphyrin dyes on TiO_2 might play a role to increase

dx.doi.org/10.1021/jp302145x | J. Phys. Chem. C 2012, 116, 11907−11916

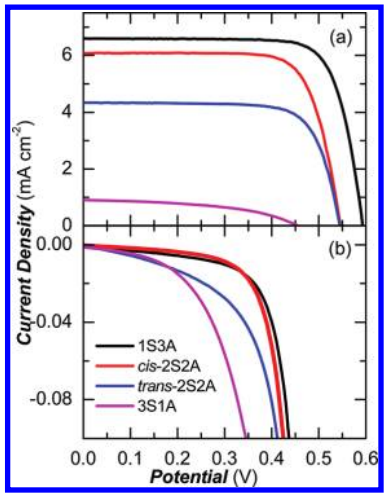

Figure 7. (a) The $I-V$ curves of 1S3A (black curve), *cis*-2S2A (red curve), *trans*-2S2A (blue curve), and 3S1A (magenta curve) sensitized solar cells under solar simulator AM1.5 light. (b) The $I-V$ curves of zinc porphyrins in the dark.

Table 2. Photovoltaic Properties of Zinc Porphyrins

Dye	J_{SC} (mA cm^{-2})	V_{OC} (mV)	*ff*	η (%)
1S3A	6.59	593	0.77	3.0
cis-2S2A	6.08	546	0.75	2.5
trans-2S2A	4.34	545	0.74	1.8
3S1A	0.907	455	0.48	0.2

the interfacial impedance depending on the degree of coverage of sensitizing dyes on the surface of TiO_2. According to the results of dye loadings, the 1S3A, *trans*-2S2A, and *cis*-2S2A give significantly higher molecular loadings on TiO_2, which behave like a blocking layer to prevent charge recombination between the electrons on TiO_2 and triiodides in the electrolyte. For 3S1A, which has a lower surface coverage on TiO_2, the triiodides in electrolyte can penetrate closely to the surface of TiO_2 to decrease the barrier for the electrons to combine with triiodides and to result in a higher dark current. On the other hand, under applied potential lower than 0.35 V, the dark current of *cis*-2S2A is smaller than that of 1S3A due to the larger amount of dye loading for the former than the latter. However, the dark current of *cis*-2S2A becomes larger than that of 1S3A over 0.35 V, which is consistent with the larger V_{OC} for 1S3A than for *cis*-2S2A. Interestingly, we found that the V_{OC} values are nearly identical for both *cis*-2S2A and *trans*-2S2A devices, even though *cis*-2S2A has a much higher J_{SC} value. On the basis of the dark current results shown in Figure 7b, charge recombination is more significant for *trans*-2S2A than for *cis*-2S2A. We thus expect that the CB edge of TiO_2 might be shifted more upward for *trans*-2S2A than for *cis*-2S2A to compensate the loss of the CB electrons of the former due to the severe charge recombination. The very poor performance of the 3S1A device can be understood for its small amount of dye loading and the very high dark current due to significant effect of charge recombination.

Figure 8 shows the spectra of conversion efficiency of incident photon to current (IPCE) of 1S3A, *cis*-2S2A, *trans*-2S2A, and 3S1A sensitized solar cells at short circuit conditions. IPCE is defined as LHE $\times$ φ_{inj} $\times$ η_{cc}, where LHE is light-harvesting efficiency depending on the absorbance of the sensitized dye, φ_{inj} is the electron injection yield depending on

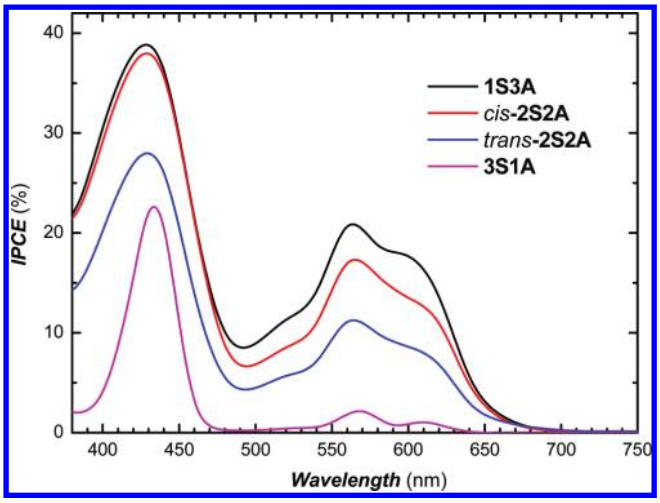

Figure 8. IPCE spectra of 3S1A (magenta curve), *trans*-2S2A (blue curve), *cis*-2S2A (red curve), and 1S3A (black curve) sensitized solar cells.

the injection rate from dye to TiO_2, and η_{cc} is the charge collection efficiency depending on the diffusion rate of electrons on TiO_2 and recombination rate between TiO_2 electrons and redox couples. Like J_{SC}, the IPCE values of four zinc porphyrins exhibit a strong correlation to the *meso*-substitutions. The IPCEs at 565 nm of zinc porphyrins are 21, 17, 11, and 2.3% for 1S3A, *cis*-2S2A, *trans*-2S2A, and 3S1A, respectively. Since IPCE is dominated by LHE (= $1-10^{-Abs}$), for which the absorbance (Abs) is a linear dependence on both the molecular loading on TiO_2 and absorption coefficient. The IPCE values at the Soret band and Q band are larger for 1S3A and *cis*-2S2A, but are much smaller for 3S1A. Noticeably, the IPCE values of 1S3A and *cis*-2S2A are similar to reach 40% at the Soret band, but at the Q band region, 1S3A exhibits a larger IPCE than *cis*-2S2A. According to the absorption spectra of zinc porphyrins/TiO_2 shown in Figure 2, the LHE of *cis*-2S2A is larger than that of 1S3A. However, the IPCE value at the Q band for *cis*-2S2A is smaller than that for 1S3A, possibly due to the smaller electron injection yield at the lowest excited state for *cis*-2S2A than for 1S3A. Moreover, the IPCE values for *cis*-2S2A at both the Soret band and the Q band are larger than those of *trans*-2S2A. We expect that, in addition to the larger amount of dye-loading to give larger LHE for *cis*-2S2A, the possibly lower CB edge of TiO_2 upon dye uptake of the *cis*-2S2A device might lead to larger electron injection rate to give greater electron injection yield for the *cis*-device than for the *trans*-device. The dark current results also show the *cis*-device to have larger η_{cc} than the *trans*-device, making an overall greater IPCE for *cis*-2S2A than for *trans*-2S2A.

■ CONCLUSION

In summary, new zinc porphyrin-based sensitizers 3S1A, *trans*-2S2A, *cis*-2S2A, and 1S3A were synthesized by the simplest possible way. It is found that the number and the position of thienyl and *p*-carboxyphenyl substituents on the zinc porphyrin dyes significantly affect the performance of the device. The study of absorption spectra on zinc porphyrins adsorbed on TiO_2 film revealed broadened absorption with aggregation characteristics especially for *cis*-2S2A and 1S3A. ATR-FTIR spectra of zinc porphyrins on TiO_2 demonstrated *meso*-*p*-carboxyphenyl-dependent chelation with a single arm binding for 3S1A and *trans*-2S2A and a double arm binding for 1S3A

dx.doi.org/10.1021/jp302145x | J. Phys. Chem. C 2012, 116, 11907−11916

and *cis*-2S2A. Overall, the position and number of bonding *p*-carboxyphenyl substitutes strongly correlated to the molecular loading on TiO_2 and modifies the charge recombination of the CB electrons with redox couples. The presence of heavy atom effect from thienyl substituents to enhance the ISC can be evidenced from the fluorescence lifetime measurements in the solution. The dark I−V measurements and the IPCE action spectra demonstrate two important factors affecting the performance of this system. One is that *meso*-*p*-carboxyphenyl substitute influences the interfacial electron interaction between trapping electrons and triiodides, and the other is that thienyl substitute alters the excited-state lifetime. The η values give an order of 1S3A (3.0%) > *cis*-2S2A (2.5%) > *trans*-2S2A (1.8%) ≫ 3S1A (0.2%).

■ ASSOCIATED CONTENT

Supporting Information

Detailed synthetic procedures and characterization data of porphyrins, normalized absorption, and emission spectra. This information is available free of charge via the Internet at http://pubs.acs.org.

■ AUTHOR INFORMATION

Corresponding Author

*E-mail: chhung@chem.sinica.edu.tw.

Notes

The authors declare no competing financial interest.

■ ACKNOWLEDGMENTS

The authors greatly acknowledge the financial support from National Science Council (Taiwan) and Academia Sinica. The help from Dr. Jiann T. Lin on the measurements and instrumentations are greatly appreciated.

■ REFERENCES

(1) Polman, A.; Atwater, H. A. *Nat. Mater.* **2012**, *11*, 174.
(2) O'Regan, B.; Gratzel, M. *Nature* **1991**, *353*, 737.
(3) Nazeeruddin, M. K.; De Angelis, F.; Fantacci, S.; Selloni, A.; Viscardi, G.; Liska, P.; Ito, S.; Bessho, T.; Gratzel, M. *J. Am. Chem. Soc.* **2005**, *127*, 16835.
(4) Wang, Q.; Ito, S.; Gratzel, M.; Fabregat-Santiago, F.; Mora-Sero, I.; Bisquert, J.; Bessho, T.; Imai, H. *J. Phys. Chem. B* **2006**, *110*, 25210.
(5) Zhang, G. L.; Bala, H.; Cheng, Y. M.; Shi, D.; Lv, X. J.; Yu, Q. J.; Wang, P. *Chem. Commun.* **2009**, 2198.
(6) Ning, Z. J.; Tian, H. *Chem. Commun.* **2009**, 5483.
(7) Imahori, H.; Umeyama, T.; Ito, S. *Acc. Chem. Res.* **2009**, *42*, 1809.
(8) Martinez-Diaz, M. V.; de la Torrea, G.; Torres, T. *Chem. Commun.* **2010**, *46*, 7090.
(9) Walter, M. G.; Rudine, A. B.; Wamser, C. C. *J. Porphyrins Phthalocyanines* **2010**, *14*, 759.
(10) Chen, C. Y.; Wang, M. K.; Li, J. Y.; Pootrakulchote, N.; Alibabaei, L.; Ngoc-le, C. H.; Decoppet, J. D.; Tsai, J. H.; Gratzel, C.; Wu, C. G.; Zakeeruddin, S. M.; Gratzel, M. *ACS Nano* **2009**, *3*, 3103.
(11) Hagfeldt, A.; Boschloo, G.; Sun, L.; Kloo, L.; Pettersson, H. *Chem. Rev.* **2010**, *110*, 6595.
(12) Yu, Q. J.; Wang, Y. H.; Yi, Z. H.; Zu, N. N.; Zhang, J.; Zhang, M.; Wang, P. *ACS Nano* **2010**, *4*, 6032.
(13) Kandavelu, V.; Huang, H. S.; Jian, J. L.; Yang, T. C. K.; Wang, K. L.; Huang, S. T. *Sol. Energy* **2009**, *83*, 574.
(14) Wang, Z. S.; Cui, Y.; Hara, K.; Dan-Oh, Y.; Kasada, C.; Shinpo, A. *Adv. Mater.* **2007**, *19*, 1138.
(15) Hara, K.; Wang, Z. S.; Sato, T.; Furube, A.; Katoh, R.; Sugihara, H.; Dan-Oh, Y.; Kasada, C.; Shinpo, A.; Suga, S. *J. Phys. Chem. B* **2005**, *109*, 15476.
(16) Kuang, D.; Uchida, S.; Humphry-Baker, R.; Zakeeruddin, S. M.; Gratzel, M. *Angew. Chem., Int. Ed. Engl.* **2008**, *47*, 1923.
(17) Horiuchi, T.; Miura, H.; Sumioka, K.; Uchida, S. *J. Am. Chem. Soc.* **2004**, *126*, 12218.
(18) Ito, S.; Zakeeruddin, S. M.; Humphry-Baker, R.; Liska, P.; Charvet, R.; Comte, P.; Nazeeruddin, M. K.; Pechy, P.; Takata, M.; Miura, H.; Uchida, S.; Gratzel, M. *Adv. Mater.* **2006**, *18*, 1202.
(19) Li, Q.; Lu, L.; Zhong, C.; Shi, J.; Huang, Q.; Jin, X.; Peng, T.; Qin, J.; Li, Z. *J. Phys. Chem. B* **2009**, *113*, 14588.
(20) Yang, C.-H.; Liao, S.-H.; Sun, Y.-K.; Chuang, Y.-Y.; Wang, T.-L.; Shieh, Y.-T.; Lin, W.-C. *J. Phys. Chem. C* **2010**, *114*, 21786.
(21) Barea, E. M.; Zafer, C.; Gultekin, B.; Aydin, B.; Koyuncu, S.; Icli, S.; Santiago, F. F.; Bisquert, J. *J. Phys. Chem. C* **2010**, *114*, 19840.
(22) Tian, H. N.; Yang, X. C.; Pan, J. X.; Chen, R. K.; Liu, M.; Zhang, Q. Y.; Hagfeldt, A.; Sun, L. C. *Adv. Funct. Mater.* **2008**, *18*, 3461.
(23) Liu, Q. S.; Jiang, K. J.; Guan, B.; Tang, Z. M.; Pei, J. A.; Song, Y. L. *Chem. Commun.* **2011**, *47*, 740.
(24) Lin, J. T.; Chen, P. C.; Yen, Y. S.; Hsu, Y. C.; Chou, H. H.; Yeh, M. C. P. *Org. Lett.* **2009**, *11*, 97.
(25) Unger, E. L.; Ripaud, E.; Leriche, P.; Cravino, A.; Roncali, J.; Johansson, E. M. J.; Hagfeldt, A.; Boschloo, G. *J. Phys. Chem. C* **2010**, *114*, 11659.
(26) Marinado, T.; Nonomura, K.; Nissfolk, J.; Karlsson, M. K.; Hagberg, D. P.; Sun, L.; Mori, S.; Hagfeldt, A. *Langmuir* **2009**, *26*, 2592.
(27) Li, G.; Jiang, K.-J.; Li, Y.-F.; Li, S.-L.; Yang, L.-M. *J. Phys. Chem. C* **2008**, *112*, 11591.
(28) Wang, Z.-S.; Li, F.-Y.; Huang, C.-H.; Wang, L.; Wei, M.; Jin, L.-P.; Li, N.-Q. *J. Phys. Chem. B* **2000**, *104*, 9676.
(29) Chen, Y.-S.; Li, C.; Zeng, Z.-H.; Wang, W.-B.; Wang, X.-S.; Zhang, B.-W. *J. Mat. Chem.* **2005**, *15*, 1654.
(30) Yum, J.-H.; Walter, P.; Huber, S.; Rentsch, D.; Geiger, T.; Nüesch, F.; De Angelis, F.; Grätzel, M.; Nazeeruddin, M. K. *J. Am. Chem. Soc.* **2007**, *129*, 10320.
(31) Won, Y. S.; Yang, Y. S.; Kim, J. H.; Ryu, J.-H.; Kim, K. K.; Park, S. S. *Energy Fuels* **2010**, *24*, 3676.
(32) Velusamy, M.; Justin Thomas, K. R.; Lin, J. T.; Hsu, Y.-C.; Ho, K.-C. *Org. Lett.* **2005**, *7*, 1899.
(33) Thomas, K. R. J.; Lin, J. T.; Hsu, Y.-C.; Ho, K.-C. *Chem. Commun.* **2005**, 4098.
(34) Trachibana, Y.; Haque, S. A.; Mercer, I. P.; Durrant, J. R.; Klug, D. R. *J. Phys. Chem. B* **2000**, *104*, 1198.
(35) Campbell, W. M.; Burrell, A. K.; Officer, D. L.; Jolley, K. W. *Coord. Chem. Rev.* **2004**, *248*, 1363.
(36) Campbell, W. M.; Jolley, K. W.; Wagner, P.; Wagner, K.; Walsh, P. J.; Gordon, K. C.; Schmidt-Mende, L.; Nazeeruddin, M. K.; Wang, Q.; Gratzel, M.; Officer, D. L. *J. Phys. Chem. C* **2007**, *111*, 11760.
(37) Lu, H. P.; Mai, C. L.; Tsia, C. Y.; Hsu, S. J.; Hsieh, C. P.; Chiu, C. L.; Yeh, C. Y.; Diau, E. W. G. *Phys. Chem. Chem. Phys.* **2009**, *11*, 10270.
(38) Bessho, T.; Zakeeruddin, S. M.; Yeh, C. Y.; Diau, E. W. G.; Gratzel, M. *Angew. Chem., Int. Ed. Engl.* **2010**, *49*, 6646.
(39) Pasunooti, K. K.; Song, J. L.; Chai, H.; Amaladass, P.; Deng, W. Q.; Liu, X. W. *J. Photochem. Photobiol. A: Chem.* **2011**, *218*, 219.
(40) Lee, C. W.; Lu, H. P.; Lan, C. M.; Huang, Y. L.; Liang, Y. R.; Yen, W. N.; Liu, Y. C.; Lin, Y. S.; Diau, E. W. G.; Yeh, C. Y. *Chem.—Eur. J.* **2009**, *15*, 1403.
(41) Wu, S. L.; Lu, H. P.; Yu, H. T.; Chuang, S. H.; Chiu, C. L.; Lee, C. W.; Diau, E. W. G.; Yeh, C. Y. *Energy Environ. Sci.* **2010**, *3*, 949.
(42) Hsieh, C. P.; Lu, H. P.; Chiu, C. L.; Lee, C. W.; Chuang, S. H.; Mai, C. L.; Yen, W. N.; Hsu, S. J.; Diau, E. W. G.; Yeh, C. Y. *J. Mater. Chem.* **2010**, *20*, 1127.
(43) Yella, A.; Lee, H.-W.; Tsao, H. N.; Yi, C.; Chandiran, A. K.; Nazeeruddin, M. K.; Diau, E. W.-G.; Yeh, C.-Y.; Zakeeruddin, S. M.; Grätzel, M. *Science* **2011**, *334*, 629.
(44) Imahori, H.; Hayashi, S.; Hayashi, H.; Oguro, A.; Eu, S.; Umeyama, T.; Matano, Y. *J. Phys. Chem. C* **2009**, *113*, 18406.
(45) Odobel, F.; Blart, E.; Lagree, M.; Villieras, M.; Boujtita, H.; El Murr, N.; Caramori, S.; Bignozzi, C. A. *J. Mater. Chem.* **2003**, *13*, 502.

(46) Liu, Y. J.; Xiang, N.; Feng, X. M.; Shen, P.; Zhou, W. P.; Weng, C.; Zhao, B.; Tan, S. T. *Chem. Commun.* **2009**, 2499.
(47) Xie, Y.; Joshi, P.; Ropp, M.; Galipeau, D.; Zhang, L. F.; Fong, H.; You, Y. J.; Qiao, Q. Q. *J. Porphyrins Phthalocyanines* **2009**, *13*, 903.
(48) Imahori, H.; Matsubara, Y.; Iijima, H.; Umeyama, T.; Matano, Y.; Ito, S.; Niemi, M.; Tkachenko, N. V.; Lemmetyinen, H. *J. Phys. Chem. C* **2010**, *114*, 10656.
(49) Hoertz, P. G.; Carlisle, R. A.; Meyer, G. J.; Wang, D.; Piotrowiak, P.; Galoppini, E. *Nano Lett.* **2003**, *3*, 325.
(50) Nazeeruddin, M. K.; Humphry-Baker, R.; Officer, D. L.; Campbell, W. M.; Burrell, A. K.; Grätzel, M. *Langmuir* **2004**, *20*, 6514.
(51) Rochford, J.; Chu, D.; Hagfeldt, A.; Galoppini, E. *J. Am. Chem. Soc.* **2007**, *129*, 4655.
(52) Alibabaei, L.; Wang, M. K.; Giovannetti, R.; Teuscher, J.; Di Censo, D.; Moser, J. E.; Comte, P.; Pucciarelli, F.; Zakeeruddin, S. M.; Gratzel, M. *Energ. Environ. Sci.* **2010**, *3*, 956.
(53) Xiang, N.; Zhou, W. P.; Jiang, S. H.; Deng, L. J.; Liu, Y. J.; Tan, Z.; Zhao, B.; Shen, P.; Tan, S. T. *Sol. Energy Mater. Sol. Cells* **2011**, *95*, 1174.
(54) Finnie, K. S.; Bartlett, J. R.; Woolfrey, J. L. *Langmuir* **1998**, *14*, 2744.
(55) Kira, A.; Matsubara, Y.; Iijima, H.; Umeyama, T.; Matano, Y.; Ito, S.; Niemi, M.; Tkachenko, N. V.; Lemmetyinen, H.; Imahori, H. *J. Phys. Chem. C* **2010**, *114*, 11293.
(56) Ma, R. M.; Guo, P.; Yang, L. L.; Guo, L. S.; Zhang, X. X.; Nazeeruddin, M. K.; Gratzel, M. *J. Phys. Chem. A* **2010**, *114*, 1973.
(57) Park, H.; Bae, E.; Lee, J. J.; Park, J.; Choi, W. *J. Phys. Chem. B* **2006**, *110*, 8740.
(58) Johansson, E. M. J.; Hedlund, M.; Siegbahn, H.; Rensmo, H. *J. Phys. Chem. B* **2005**, *109*, 22256.
(59) Lee, C. Y.; She, C. X.; Jeong, N. C.; Hupp, J. T. *Chem. Commun.* **2010**, *46*, 6090.
(60) Park, J. K.; Lee, H. R.; Chen, J. P.; Shinokubo, H.; Osuka, A.; Kim, D. *J. Phys. Chem. C* **2008**, *112*, 16691.
(61) Pellegrino, G.; Condorelli, G. G.; Privitera, V.; Cafra, B.; Di Marco, S.; Alberti, A. *J. Phys. Chem. C* **2011**, *115*, 7760.
(62) Park, J. K.; Chen, J. P.; Lee, H. R.; Park, S. W.; Shinokubo, H.; Osuka, A.; Kim, D. *J. Phys. Chem. C* **2009**, *113*, 21956.
(63) Koumura, N.; Wang, Z.-S.; Mori, S.; Miyashita, M.; Suzuki, E.; Hara, K. *J. Am. Chem. Soc.* **2006**, *128*, 14256.
(64) Chen, C.-Y.; Wu, S.-J.; Wu, C.-G.; Chen, J.-G.; Ho, K.-C. *Angew. Chem., Int. Ed.* **2006**, *45*, 5822.
(65) Wang, Q.; Carnpbell, W. M.; Bonfantani, E. E.; Jolley, K. W.; Officer, D. L.; Walsh, P. J.; Gordon, K.; Humphry-Baker, R.; Nazeeruddin, M. K.; Gratzel, M. *J. Phys. Chem. B* **2005**, *109*, 15397.
(66) Papageorgiou, N.; Maier, W. F.; Gratzel, M. *J. Electrochem. Soc.* **1997**, *144*, 876.
(67) Eu, S.; Hayashi, S.; Umeyama, T.; Oguro, A.; Kawasaki, M.; Kadota, N.; Matano, Y.; Imahori, H. *J. Phys. Chem. C* **2007**, *111*, 3528.
(68) Heredia, D.; Natera, J.; Gervaldo, M.; Otero, L.; Fungo, F.; Lin, C. Y.; Wong, K. T. *Org. Lett.* **2010**, *12*, 12.
(69) Tian, H. N.; Yang, X. C.; Chen, R. K.; Zhang, R.; Hagfeldt, A.; Sunt, L. C. *J. Phys. Chem. C* **2008**, *112*, 11023.
(70) Abbotto, A.; Manfredi, N.; Marinzi, C.; De Angelis, F.; Mosconi, E.; Yum, J. H.; Zhang, X. X.; Nazeeruddin, M. K.; Gratzel, M. *Energy Environ. Sci.* **2009**, *2*, 1094.